Hindawi
Shock and Vibration
Volume 2018, Article ID 2506909, 12 pages
https://doi.org/10.1155/2018/2506909

*Research Article*

# The Influence of the Track Parameters on Vibration Characteristics of Subway Tunnel

**Wenbo Shi**,[1,2] **Linchang Miao**,[3] **Junhui Luo**,[4] **and Honglei Zhang**[5]

[1]*School of Traffic and Transportation, Xuchang College, Xuchang 461000, China*
[2]*Henan Small and Medium-Sized Cities Public Transport Information Engineering Research Center, Xuchang 461000, China*
[3]*Institute of Geotechnical Engineering, Southeast University, Nanjing 210018, China*
[4]*Guangxi Communications Planning Surveying and Designing Institute Co., Ltd., Nanning 530029, China*
[5]*Henan Zhibo Architectural Design Group Co., Ltd., Xuchang 461000, China*

Correspondence should be addressed to Wenbo Shi; shwanbe@163.com and Linchang Miao; lc.miao@seu.edu.cn

Received 13 March 2018; Revised 23 May 2018; Accepted 19 June 2018; Published 18 October 2018

Academic Editor: Elena Dragomirescu



In soft soil areas, such as the Nanjing, it is very important to quantitatively analyze the dynamic behaviors of soft soils during the metro train operation. A nonlinear coupling model of wheel-track and a finite element calculation model of tunnel and soil were established based on the mechanical character of elastic supporting block ballastless track and the actual parameters of Nanjing soft soil. The time-variant vertical acceleration of the rail, the sleepers, and the surface of the tunnel can be calculated by the models, and the frequency dependence acceleration was verified by the fast Fourier transform algorithm. A modified vibration power level for human sensitivity was used to quantify the vibration energy of each part of the system, and the impact of the parameters in the model was evaluated. The results can be applied to the metro design and construction, which also can be the guidance during the tunnel construction.

## 1. Introduction

With the continuous development of urbanization, the urban traffic is getting increasingly crowded. It is turning into the biggest chronic disease of the cities [1], which consists of traffic congestion, fog and haze weather, vehicle noise, and so on, and the subway is a best way to solve it. The metro that plays an important role in the modern life begins to spring up in many cities of China, and it shows a fast, convenient, and environment-friendly way. China's metro construction is entering a new period when both the construction speed and scale are first in the world, with 94 lines in operation, 120 lines in construction, and over 150 billion gross investment [2]. However, the vibrations induced by the high-speed moving metro trains for the surrounding metro lines will become a significant problem which has to be solved.

The research studies, which include metro vehicle and track coupling system and vibration energy transform in the soil, usually consist of two independent sections. Studies on vehicle-track dynamics have been performed for a long time in many countries through the establishment of coupling model. Timoshenko [3] presented to use the frequency-domain technique to analyze track dynamics with continuously supported Euler beam. Xu et al. [4] established the vehicle/track interaction model, which can be used to reveal the interaction mechanisms between the moving vehicles and the guiding tracks. Aggestam et al. [5] evaluated the wheel-rail contact forces, bending moments in the concrete panel and load distributions on the supporting foundation by two generic slab track models including one or two layers of concrete slabs. Lopes et al. [6] focused on the experimental validation of a numerical approach previously proposed for the prediction of vibrations inside buildings due to railway traffic in tunnels. Three autonomous models compose the numerical model in order to simulate the generation, propagation, and reception of vibrations. Studies in recent years have been a trend to regard the vehicle and track model

as an integral system on dynamics of wheel-rail interactions [7–12].

Research that focused on the propagation of vibration caused from the wheel-rail exceeding in the soil has also been developed many years in the world. The models, which used to solve the problem of vibration wave propagation in the soil caused by metro operation, can be classified into two categories: the finite element models (FEMs) and analytical method. Analytical method is confined by many hypotheses, like supposing the soil material as elastic continuum material, supposing the load applied on the tunnel is harmonic in both space and time, and so on. Forrest and Hunt [13] described a three-dimensional model for the dynamics of a deep underground railway tunnel in infinite soil, and the ground vibration due to excitation by running trains in frequency 20 to 100 Hz was analyzed. Bian et al. [14] used a 2.5D FEM formulation with viscous artificial boundaries to model wave propagation from underground moving loads. The periodic 2.5D FEM models for the dynamic simulation of tunnels have been extensively applied to simulate the dynamic interaction between soil and tunnel structures [15, 16]. Many models established in research papers above assumed radius of the model from the center of the tunnel increases towards infinity in every direction; therefore, it can not calculate the remnant vibration energy transform to the surface of the soil. The subway operation problem is clearly a moving load problem, and some elegant solutions in FEM appear in the literature. Amado-Mendes et al. [17] devised the subway finite element model to determine the dynamic stress and analyzed dynamic response under vibration loading. The relationship between the train speed and the vibrations on the track with a FEM model is studied by El Kacimi et al. [18]. Gardien and Stuit [19] established a modular model that consists of static deflection model, track model, and the propagation model, and the effect of change element size, soil stiffness, damping, and boundary conditions is analyzed. Ekevid et al. [20] described in detail the mesh refinement and coarsening in the case of HST applications, with successful validations. Ju [21] investigated the characteristics of building vibrations induced by adjacent moving trucks using finite element analyses. Regarding urban traffic, research is scarcer. Andersen and Jones [22] investigated the quality of the results obtained from a 2D-coupled FE-BE model comparing it with a 3D-coupled FE-BE model. Real et al. [23] developed a 3D numerical FEM model of a railway tunnel to predict railway-induced vibrations. Vogiatzis [24] studied the effect of ground-borne vibrations generated by underground metro and their effects on ancient monuments.

The research of the subway system mostly focused on the vibration damping track, and the vehicle-wheel coupling system was established; the effect on the environment by subway vibration was discussed through field measurement and data fitting during the metro operation. Quantitatively analyzing each parameter's influences, which focused on system vibration energy causing and spreading, is particularly important through establishing a vehicle-rail-sleeper-ballast-lining-soil body model. The subway tunnel buried in a soft soil area will have a big settlement, which is caused by the vibration energy of vehicle long cycle action during the process of vehicle operation, because the soft clay has the characteristics of high water content, big compressibility, and low intention. The practical engineering shows that the subsidence generated approximately 16 cm of Shanghai metro line 1 during the metro long-term operation, and the largest subsidence near the Helen Road station has reached 30 cm [25], and thus, analyzing the effect of track parameters on the vibration energy generate and transform in soft soil area has important implications.

## 2. Vehicle-Track Coupling Model

The settlement of the soft soil surrounding along metro lines is caused by the long-term cyclic loading during the metro operation. The magnitude of settlement mainly depends on the force at the vehicle-track contact and the vertical vibration acceleration of the system; thus, how to reduce the effect of the vibration becomes a key, which can decrease the soil settlement. Considering the vehicle leading and trailing bogie symmetrically arranged in general, and the ups and downs of vibration of car body with nodding vibration will not cause coupling, the half car body model is established, which is based on the geometric characteristics of the elastic supporting block ballastless track, as shown in Figure 1.

## 3. The Vehicle Model of the Metro Train

As shown in Figure 1, $M_c$, $M_t$, and $M_w$ stand for the quality of half train body, the bogie, and the wheel set, respectively; $J_t$ is nod inertia of the body's frame; $K_{sz}$ and $K_{pz}$ is the stiffness of the vehicle primary and secondary suspension; $C_{sz}$ and $C_{pz}$ is the damping of the vehicle primary and secondary suspension; and $z_1$ and $z_2$ are, respectively, for the location of the wheel-rail contact irregularity. Vibration equation about the upper part of the vehicle model is established according to the Hamilton principle as follows:

$$[M_u]\{\ddot{u}\} + [C_u]\{\dot{u}\} + [K_u]\{u\} = \{P_u\}. \quad (1)$$

## 4. The Track Model of the Metro

The elastic supporting block ballastless track is supported by rail, fasteners, concrete supporting block, rubber pads under supporting block, rubber boots, concrete track bed, etc., and the track's vertical stiffness and damping is mainly provided by the fasteners and the piece of rubber pad. These components of the model can use the stiffness and damping parameters to describe them, such as, $K_r$, $C_r$ and $K_s$, $C_s$, respectively. Thus, acceleration of vibration of the elastic supporting block ballastless track is mainly reflected on the rail and concrete supporting block.

Newton and Clark [26] analyzed the impact on the vehicle-track coupling nonlinear system with assuming track for Euler beam and Timoshenko beam, respectively. The results showed that the Timoshenko beam has a higher accuracy when analyzing the rail shear stress; however, the computational time was higher for the Timoshenko beam. This paper uses the Euler model because the two beams have little difference in accuracy in the analysis of the vertical

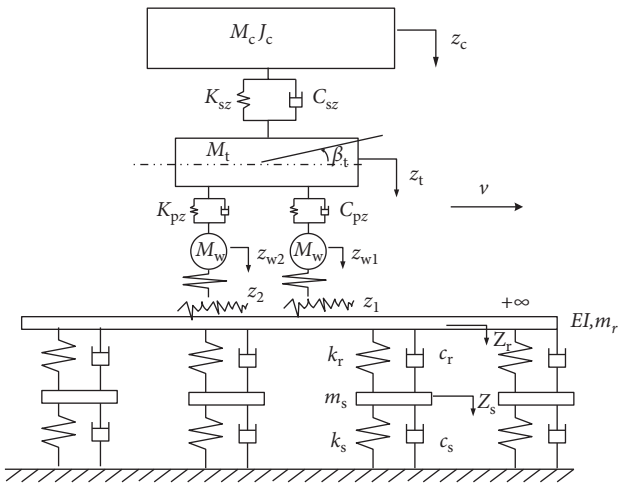


Figure 1: The half-vehicle-track coupled nonlinear model.

vibration displacement of the track. The differential equation of rail vibration deformation under the relevant knowledge of mechanics of materials is as follows:

$$EI\frac{\partial^4 Z_r(x,t)}{\partial x^4} + m_r\frac{\partial^2 Z_r(x,t)}{\partial t^2} = -\sum_{i=1}^{N} F_{rsi}(t)\delta(x-x_i) + \sum_{j=1}^{2} p_j(t)\delta\left(x-x_{wj}\right), \tag{2}$$

where $F_{rsi}(t) = K_{pi}[Z_r(x_i,t) - Z_{si}(t)] + C_{pi}[\dot{Z}_r(x_i,t) - \dot{Z}_{si}(t)]$, $\delta$ is the Dirac function, $Z_{si}(t)$ is the sleeper vibration displacement, $F_{rsi}$ is the reaction supporting force of the $i$th root sleeper, and $p_j$ is the wheel-rail coupling force at the sites of $j$th wheels.

The vibration equation on sleeper is as follows:

$$K_p\left[Z_r(x_i,t) - Z_{si}(t)\right] + C_p\left[\dot{Z}_r(x_i,t) - \dot{Z}_{si}(t)\right] - K_b Z_{si}(t) - C_b\dot{Z}_{si}(t) = M_{si}\ddot{Z}_{si}(t). \tag{3}$$

Assumptions on the two ends of the rail are simply supported, the boundary conditions for the moment can be obtained, and the displacement of the rail and bending moment on the cross section is zero at $x = 0$ [27, 28].

The corresponding characteristic function, namely, the free vibration modal is as follows:

$$Y_r(x) = C_1 \sin\frac{r\pi x}{l} \quad (r = 1, 2, \ldots). \tag{4}$$

By orthogonal processing of the characteristic function by $\int_0^L mY_r^2(x)dx = 1$, it can be obtained that $C_1 = \sqrt{2/ml}$, and then the free vibration modal equation is as follows:

$$Y_r(x) = \sqrt{\frac{2}{ml}}\sin\frac{r\pi x}{l} \quad (r = 1, 2, \ldots). \tag{5}$$

So

$$Z_r(x_i,t) = Y(x)q(t) = \sqrt{\frac{2}{m_r l}}\sin\frac{k\pi x}{l}q_k(t). \tag{6}$$

Simplifying the track nonlinearity equations by substituting Equation (6) into Equations (2) and (3), the final vibration equation is as follows:

$$[M_1]\{\ddot{q}\} + [C_1]\{\dot{q}\} + [K_1]\{q\} = \{P_1\}. \tag{7}$$

The enough mode number is the guarantee to be the precision in the process of solving the vibration equation of the track by using the modal analysis method [29]. The results of numerical calculations show that the calculation accuracy can well meet the requirements if the mode number is greater than $0.5\,L/L_s$, where $L$ is the rail length and $L_s$ is the distance of the adjacent sleepers.

## 5. Nonlinear Contact Stress Calculation of the Wheel-Track

The wheel-track contact stress can be calculated based on Hertz nonlinear contact theory, and the wheel-track vertical force is as follows:

$$p(t) = \left[\frac{1}{G}\delta_{Z(t)}\right]^{3/2}, \tag{8}$$

where $G$ is the wheel-rail contact constant, a wheel-rail contact constant's empirical formula for a contact constant is $G = 4.57R^{-0.149} \times 10^{-8}$, and $\delta_{Z(t)}$ is for elastic compression between the wheel and track.

It can be very well to connect the upper vehicle model and the lower track model, which made them as a complete system with Equation (8).

## 6. The Newmark Integration Method

Time-stepping integration provides the best way for a numerical solution of the equations of motion of the vehicle-track system including nonlinearities. Writing the vehicle vibration equation and the track vibration equation in a same way is shown in the following equation:

$$[M]\{\ddot{x}\} + [C]\{\dot{x}\} + [K]\{x\} = \{P\}. \tag{9}$$

The useful approach to calculate these equations is the method of the Newmark explicit iterative which is used widely in engineering practice. Assuming that $\{\ddot{x}\}_{t-1}$, $\{\dot{x}\}_t$, and $\{x\}_t$ are known at time $t$, in $t + \Delta t$ moment, the equation solution can be expressed as follows:

$$\begin{cases} \{x\}_{n+1} = \{x\}_n + \{\dot{x}\}_n\Delta t + \left(\frac{1}{2} + \psi\right)\{\ddot{x}\}_n\Delta t^2 - \psi\{\ddot{x}\}_{n-1}\Delta t^2, \\ \{\dot{x}\}_{n+1} = \{\dot{x}\}_n + (1+\varphi)\{\ddot{x}\}_n\Delta t - \varphi\{\ddot{x}\}_{n-1}\Delta t, \end{cases} \tag{10}$$

where $\Delta t$ is the time step and $\psi$ and $\varphi$ are free parameters which control the stability and numerical dissipation of the algorithm. The next step vibration expression can be written as shown in Equation (11) by substituting the above solving method with initial condition into the system vibration equation:

$$[M]\{\ddot{x}\}_{n+1} + [C]_{n+1}\{\dot{x}\}_{n+1} + [K]_{n+1}\{x\}_{n+1} = \{P\}_{n+1}. \tag{11}$$

For each time step, calculate the displacements and velocities of the vehicle calculate model (1) and the track calculate model (7) with the Newmark integration method, and

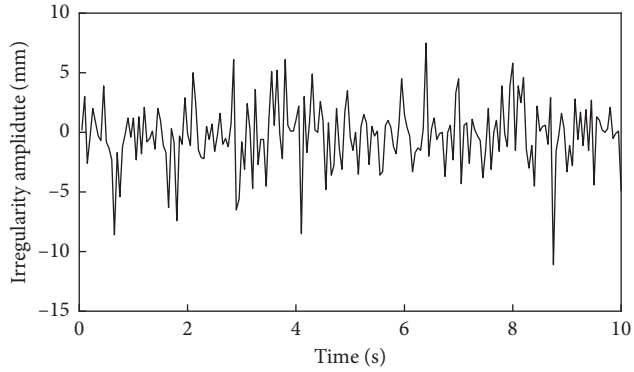


Figure 2: Track random irregularity.

Table 1: Vehicle parameters in specific value.

| Quantity | Half vehicle quality ($M_c$) | Bogie quality ($M_t$) | Bogie pitch moment of inertia ($J_t$) | Wheel quality ($M_w$) | Primary suspension stiffness ($K_{sz}$) | Primary suspension damping ($C_{sz}$) | The second suspension stiffness ($K_{pz}$) | The second suspension damping ($C_{pz}$) | Half of bogie wheelbase ($l_h$) |
|---|---|---|---|---|---|---|---|---|---|
| Value | 38500 kg | 2980 kg | 3605 kg/m$^2$ | 1350 kg | $2.14\times10^6$ N/m | $4.9\times10^4$ N·s/m | $2.535\times10^6$ N/m | $1.96\times10^5$ N·s/m | 1.2 m |

the nonlinear wheel-track contact forces can then be determined based on the calculated Equation (8). With these known results, the accelerations of the vehicle and the track are finally calculated from each equation of motion.

## 7. Applying of the Stochastic Irregularity

In general, the stochastic irregularity in the vehicle-track modelling is used to represent the vehicle travel state because of the nondeterministic excitation in the wheel-track system. As the rail surface geometry is influenced by many complex factors, these effects caused by the track irregularity have obvious randomness. The spectrum density function of the metro track for line grade six from America Railway Standard is used in this calculation. The simulation using trigonometric series method converts track irregularity power spectrum to the time domain excitation function which applied to the system as a random excitation. The final amplitude curves of vertical track irregularity is shown in Figure 2.

## 8. The Result Solutions of the Vehicle-Track Coupled Model

The parameters adopted for computing system at Section 1 are listed in Tables 1 and 2.

The speed of the metro vehicle is 40–80 km/h in a general way, and the faster the speed is, the bigger the wheel-track contact force is. In this calculation, the speed of the vehicle is set to 80 km/h. According to the vehicle-track nonlinear coupled calculation model shown at Section 1 and the parameter values shown at Tables 1 and 2, the displacement of the sleeper in the process of metro vehicle driving can be basically in agreement with the Newmark integration method. Priest and Powrie [30] used geophones to measure the sleeper's displacement during train service and used a modified beam on an elastic foundation method (BOEF) to calculate the displacement of the sleeper. The time domain result is shown in Figure 3.

These show similar behavior of the sleeper displacement during the operation in Figure 3. The calculation of vehicle-track coupled model is closer to the measured one when compared with BOEF method; nevertheless, the decay of the displacement is slower than BOEF method because of the characteristic of the modal analysis.

The accuracy of the vibration prediction depends on the chosen input parameters in the system. The vehicle-track nonlinear coupling system can be used to analyze the influence of the parameters' change on the system vibration, including vehicle speed, the stiffness and damping of the fastener and the rubber pad, random irregularity, and wave depth. Nevertheless, the most easily implemented measure is to adjust the stiffness and damping of the fastener and the rubber pad for the engineering practice. Thus, analysis effect of the stiffness and damping of the fastener and the rubber pad will play a key role in the vibration-controlling technique design of the practical engineering.

According to the nonlinear-coupled system established earlier, the rail and sleeper vibration acceleration in time domain can be obtained in the process of metro vehicles driving shown in Figures 4 and 5 shows the acceleration power spectrum density of the rail and sleeper vibration.

Figures 4 and 5 show that the acceleration amplitude of the rail vibration is bigger than the sleeper, which illustrates the energy of vibration attenuated in the spread of rail, fasteners, sleeper, and the rubber pad. Thus, the quantitative analysis of track parameters is of great significance for vibration energy transmission system.

Single bogie is able to be applied for the qualitative analysis of influence on vibration generation and attenuation during its transform by parameter change.

Table 2: Wheel coupling system orbit parameters in specific value.

| Quantity | The quality of the rail unit length ($m_r$) | Rail elastic modulus ($E$) | Rail section inertia ($I$) | Fastener vertical stiffness ($K_r$) | Fastener damping ($C_r$) | Sleeper quality ($m_s$) | The sleeper spacing ($a$) | Under the sleeper rubber pad stiffness ($K_s$) | Under the sleeper rubber pad damping ($C_s$) | C40 concrete elastic modulus ($E_c$) | Concrete Poisson's ratio ($\nu$) |
|---|---|---|---|---|---|---|---|---|---|---|---|
| Value | 60 kg/m | $2.059\times10^{11}$ Pa | $2.037\times10^{-5}$ m$^4$ | $7.8\times10^{7}$ N/m | $5\times10^{4}$ N·s/m | | 0.545 m | $7.8\times10^{7}$ N/m | $5.88\times10^{4}$ N·s/m | $3\times10^{10}$ Pa | 0.2 |

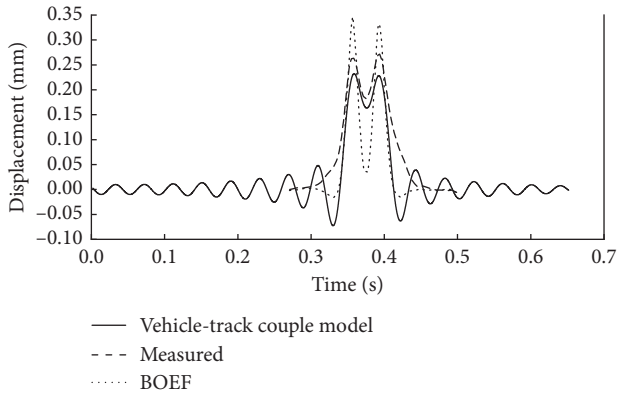


Figure 3: Comparison of measured sleeper displacement with that obtained from using the vehicle-track coupled model and BOEF model for a single bogie.

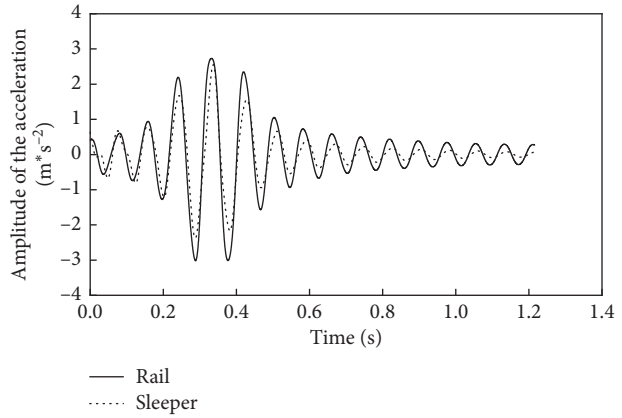


Figure 4: Rail and sleeper vibration acceleration time-domain amplitude.

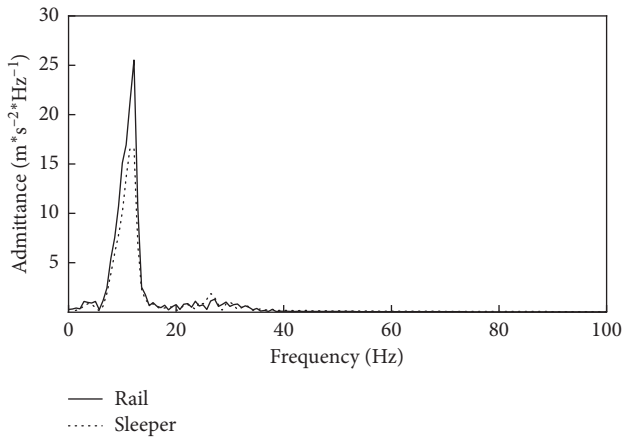


Figure 5: Rail and sleeper vibration acceleration amplitude in frequency domain.

The magnitude of the vertical load on tunnel can be calculated according to Equation (12), and the result is shown in Figure 6

$$P = Z_s K_s + V_s C_s. \tag{12}$$

## 9. The Introduction of the Modified Vibration Power Level Index

The modified vibration power level index is used to quantify the sense of the human body for the environmental vibration and to clearly recognize the harm to human body by vibration. According to the recommendations in International Standards Organization (ISO2631), the most sensitive human body to vibration frequency is mainly concentrated in the domain of 1–80 Hz, meanwhile the human body responds to the vibration of different directions shown in Figure 7.

Based on the investigations of International Standards Organization, human body sensitive degree is different to the vibration of different frequency ranges [31]. The modified vibration power level is an index to evaluate the influence of vibration on human by amending the effective amplitude of acceleration based on human reactivity, and the unit of the modified vibration power level is dB, which shows the logarithmic ratio of vibration energy. The definition of vibration energy index formula is as follows:

$$L_e = 20 \log \frac{a_e}{a_0}, \tag{13}$$

where $a_0 = 1 \times 10^{-6}\,\mathrm{m/s^2}$ and $a_e$ is the correction of acceleration RMS, and the specified solving equation is as follows:

$$a_e = \sqrt{\sum a_n^2 \cdot 10^{C_n/10}}, \tag{14}$$

where $a_n$ is the effective acceleration amplitude for $n$ Hz and $C_n$ is the modification value according to the human response to vibration, as shown in Figure 7, and the specific value is given in Table 3.

The rail and sleeper vibration acceleration amplitude in time domain can be calculated according to the vehicle-track coupling nonlinear model presented in this paper; and then its power spectral density amplitude is obtained by the fast Fourier transform. However, the analysis of the data often adopts the method of 1/2 octave bands to the calculation of modified vibration power level. The standard of 1/2 octave bands is the number of center frequency in multiples of 2 of the center frequency, and modified vibration power level of human feeling can be obtained by the sum of vibration energy in each center frequency range. And the vibration virtual value of acceleration in each center frequency bandwidth, namely, $a_n$, is the vibration acceleration root-mean-square in the frequency domain, and its expression is as follows:

$$a_n = \sqrt{a_1^2 + a_2^2 + a_3^2 + \cdots}. \tag{15}$$

Therefore, the influence of each parameter of the system on the vibration performance can be calculated by the modified vibration power level in the proposed model, and the quantified analysis effect on the system vibration of different parameters has come true by this way.

By using the above method, specific figures of the system vibration power level affected by the change of parameters in

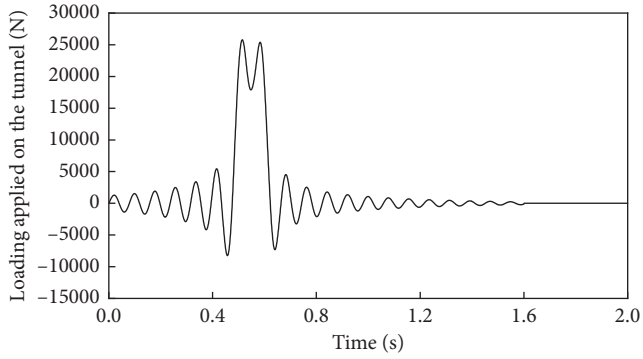


Figure 6: Vertical load applied on the tunnel shell.

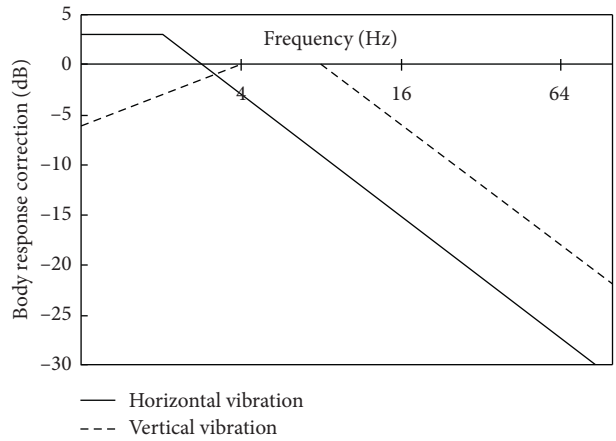


Figure 7: Human body response to different direction vibration.

Table 3: Modification value of vertical effective acceleration within the center frequency.

| 1/2 octave bands center frequency (Hz) | 1 | 2 | 4 | 8 | 16 | 31.5 | 63 | 90 |
|---|---|---|---|---|---|---|---|---|
| Vertical modified vibration power level (dB) | −6 | −3 | 0 | 0 | −6 | −12 | −18 | −21 |

the vehicle-track coupled model can be collected; the result is shown in Figures 8 and 9.

The result shows that the track vibration power level reduces nearly 23 dB when the stiffness of fastener increases from $0.5 \times 10^7$ N/m to $100 \times 10^7$ N/m, but vibration power level of the sleeper reduces less than 2 dB. Similarly, track vibration power level will decrease 6 dB when damping of the fastener increases from $0.5 \times 10^4$ N·s/m to $50 \times 10^4$ N·s/m and vibration power level of the sleeper reduces nearly 2 dB.

Changing stiffness and damping of the fastener have great influence on the vibration performance of rail, but the effect of the vibration of the sleeper damping is small. Meanwhile, stiffness change of the fastener has better consequence on vibration attenuation. However, it is bound to reduce deformation of the track caused by vibration and to restrict the development of the long wave acceleration if the stiffness of the fastener is blindly increased. In addition, the stiffness of the fastener that is increased will lead to the increment of the wheel-track coupling force and the generation of noise.

Figures 10 and 11 show that the track vibration power level reduces 25 dB and the sleeper vibration power level decreases more than 45 dB when the stiffness of the under sleepers' rubber pad also increases from $0.5 \times 10^7$ N/m to $100 \times 10^7$ N/m. At the same time, the vibration power level of the rail will be reduced nearly 7 dB and sleeper vibration power level will be lost about 4 dB when the damping of the rubber pad increased from $0.5 \times 10^4$ N·s/m to $50 \times 10^4$ N·s/m. Thus, it can be seen that increasing the stiffness of fastener and under sleeper rubber pad can significantly reduce the rail and sleeper vibration power level. The vibration of the subgrade is small in elastic supporting block ballastless track system, so the influence of the stiffness and damping of rubber pad which at the bottom of the system on the vibration characteristics is bigger.

Rail and sleeper vibration energy are basic agreement when the stiffness of the rubber pad is relatively small. The main reason is that the lower rigidity leads to large deformations of the rubber pad when the overlying load transfers to it and the stiffness increment of the fasteners cannot be able to play its role

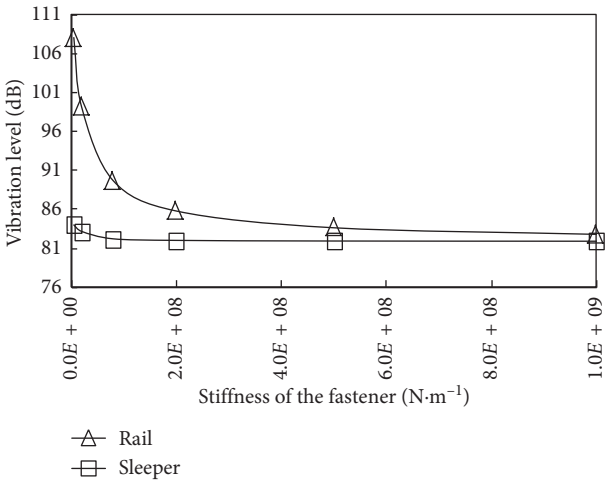


Figure 8: The influence of stiffness of fastener on the vibration power level.

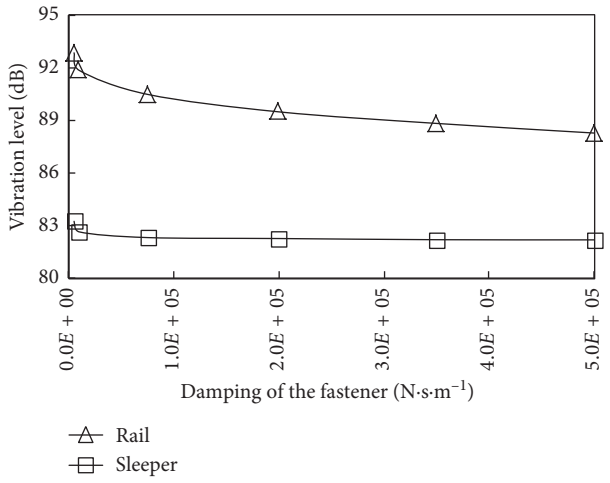


Figure 9: The influence of damping of fastener on the vibration power level.

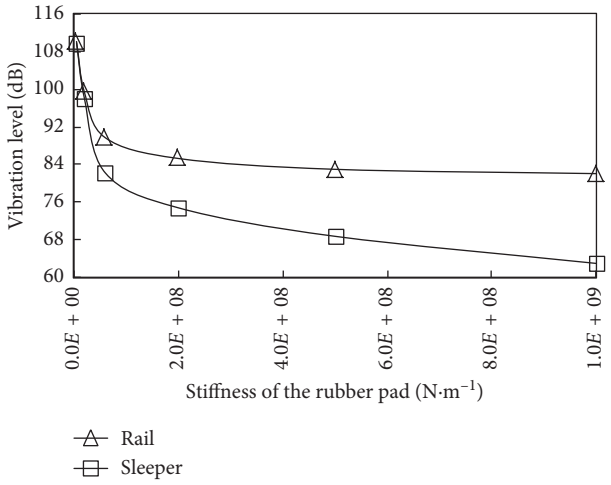


Figure 10: The influence of stiffness of the rubber pad on the vibration power level.

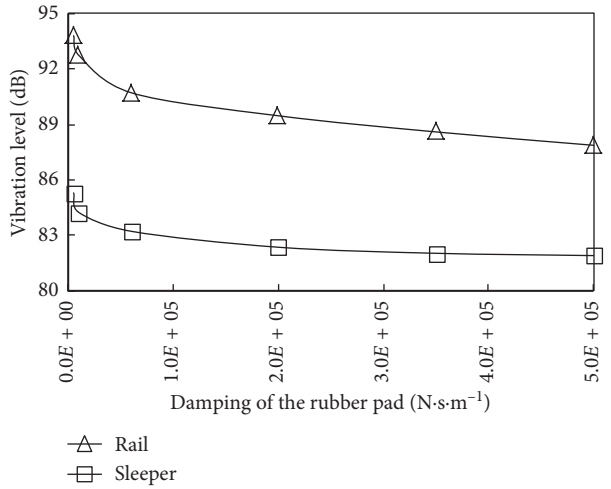


Figure 11: The influence of damping of the rubber pad on the vibration power level.

in the system. The small stiffness of the rubber pad made the structure on it to form an integral whole when the large vibration load transfers from the rail to here.

In the whole vehicle-track system, the effect of the stiffness and damping of the fastener will gradually appear when the stiffness of the rubber pad increases, the difference of the rail and sleeper vibration energy amplitude gradually expend as shown in Figure 10. The deformation is small which is caused by the vehicle-track exciting force when the stiffness of the rubber pad is increased to a greater value under low frequency arrange. Thus, the vertical vibration speed of the sleeper will be decreased as the damping of the sleeper increased, which will also reduce strain velocity of the track and then affect its vibration energy change.

## 10. The Finite Element Modelling

Vibration will generate because of track irregularity during the metro operation. The vibration energy passes onto the soil via rail, sleeper, track ballast, and tunnel lining, and it has great impact on the construction and residents' life when it transfers to the subway tunnel surface; therefore, the analysis of the change of damping and stiffness of the fastener and sleeper rubber pad is of great significance to the influence of vibration energy spreading to the surface.

The finite element method is used to calculate the acceleration of an arbitrary point in the soil due to an operation vehicle. The superiority of the finite element method is to analyze the interaction between the tunnel segments and the surrounding soft soil, and the subroutine can be used to simulate the soil to ensure the validity of the result calculated in the model.

According to the size of elastic supporting block ballastless track, the finite element model was established. Generally, the size of mesh must be at least 1/8th wavelengths to ensure calculated precision when meshing the finite element model [32]. The size of mesh should be around 2.4 m because the nature frequency of vibration in Nanjing soft soils is 10–80 Hz and the speed of stress wave is 190 m/s,

and the finite element model is set up as shown in Figure 12. The model boundary conditions are symmetrical layout along the tunnel axis, and at the bottom, the right-hand, and the left-hand, the viscous-spring boundary conditions are applied. The viscous-spring boundary conditions made the model seem like an infinite layered half-space, and the vibration energy will decay to zero and without any reflections. The connection between tunnel lining and subgrade is set as surface-to-surface contact, the normal behavior is "hard" contact, and the tangential behavior is friction contact, which may simulate the mechanical relationship between lining and subgrade well. The connection between surrounding soil and tunnel lining is set as Tie [33].

The exciting force is calculated by the vehicle-track coupled model shown in Figure 6. The load applied on the subgrade of the finite model systematically during the metro operation is shown in Figure 13, and the vibration acceleration of an arbitrary point can be computed during the vehicle operating.

The finite element model of the metro tunnel is made up of track bed slab, subgrad, and tunnel lining, and supposing these components are liner-elastic material. In the simulate calculation, the track bed slab and subgrad using C40 concrete which value is shown in Table 4, and the tunnel lining uses concrete labeled C55, and the value is shown in Table 5.

The clay is the soft soil of Nanjing of China for the finite element model calculation. The samples were sampled by thin-wall soil samples from the site of Nanjing metro 4 line, and the sampler is cylindrical for 30 cm high and 11 cm diameter, as shown in Figure 14. The dynamic triaxial tests are constructed by the GDS system shown in Figure 15. The GDS dynamic triaxial system can do the real-time monitoring during the tests; therefore, test data can be recorded and accessed in high speed. The calculation parameters of the soft soil for the segment-soil interaction-coupled model are measured under cyclic load of 75 kPa, 1 Hz frequency, and 5000 load cycles, and the specific value of the parameters are shown in Table 6.

According to the stress-strain curves based on the hyperbolic shape established by Hardin and Drnevich [34], setting up the functional relationships between the dynamic elastic modulus and dynamic strains is shown in Figure 16:

$$E_d = \frac{E_0}{1 + (\varepsilon_d/\varepsilon_r)}. \tag{16}$$

According to the result of the experiment, we got the parameter values for Nanjing soft clay: $E_0 = 47.2$ and $\varepsilon_d = 0.038$. Dynamic elastic modulus is used in the finite element software, and the quantitative influence of material parameters of fastener and under sleeper rubber pad on vibration energy transform in the soft soil to the surface of the earth is studied. The acceleration of the surface is calculated by the finite model is shown in Figure 17.

By changing the stiffness of the fastener and sleeper, the calculation results are shown in Figures 18 and 19, respectively.

The fact can be found that the surface vibration power level of the stiffness change of fastener and sleeper is obvious more than the change of the damping of them from Figures 18 and 19. Meanwhile, the impact of changing the stiffness of sleeper rubber pad is the largest and the vibration power level of the surface reduces 2.5 dB when the stiffness increased from $0.5 \times 10^7$ N/m to $100 \times 10^7$ N/m, while the change of the other parameters is not significantly affected at the surface vibration power level.

Vibration energy continuously decays during the spread through rail, sleeper, ballast bed, lining, and the soil, as shown in Figure 20. It decays almost 9% when transferring from rail to sleeper and attenuates 20% when passing on to the tunnel lining, while vibration level reduces nearly 38% when vibration energy finally transfers to the surface of the ground.

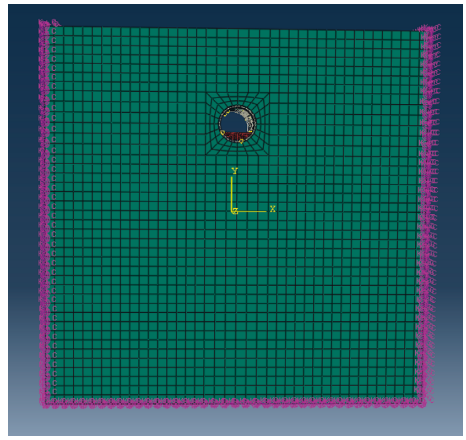

Figure 12: The finite model of the metro tunnel.

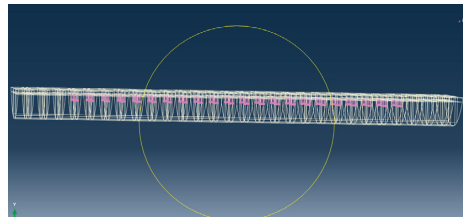

Figure 13: The load applied on the finite model.

Table 4: Track bed slab and subgrad parameter values.

| Quantity | Young's modulus ($E$) | Poisson's ratio ($\nu$) | Density ($\rho$) |
|---|---|---|---|
| Value | $3.25 \times 10^{10}$ Pa | 0.2 | 2450 kg/m$^3$ |

## 11. Conclusion

The parameters of fastener and sleeper rubber pad influences on the system vibration characteristics are analyzed in this paper by establishing wheel-track nonlinear coupling dynamic model and the finite element model, specifically:

(1) The vibration energy indicator combined with human sensitivity is introduced to research the vibration characteristics of the system, and the results can be more intuitive to show the influence of various parameters on the system vibration characteristics.

Table 5: Tunnel lining parameter values.

| Quantity | Young's modulus ($E$) | Poisson's ratio ($\nu$) | Density ($\rho$) | Inner diameter ($a$) | Thickness of the tunnel shell ($h$) |
|---|---|---|---|---|---|
| Value | $3.45 \times 10^{10}$ Pa | 0.17 | 2450 kg/m$^3$ | 2.7 m | 0.3 m |

Figure 14: Cylindrical samples.

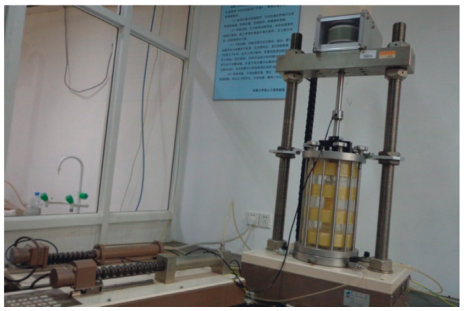

Figure 15: GDS test system.

Table 6: The parameter of the soil.

| Quantity | Poisson's ratio ($\nu$) | Density ($\rho$) | Pressure wave velocity ($c_1$) | Shear wave velocity ($c_2$) | Volumetric damping ($\eta_K$) | Hysteretic loss factor ($\eta_G$) |
|---|---|---|---|---|---|---|
| Value | 0.3 | 1859 kg/m$^3$ | 524 m/s | 190 m/s | 0 | 0.06 |

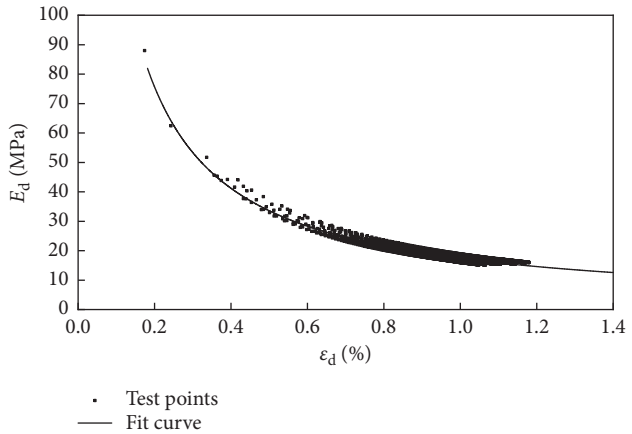


Figure 16: The relationship between dynamic elastic modulus and dynamic strains.

(2) Increasing the stiffness and damping of fastener and under sleeper rubber pad can make a direct result of rail, sleeper vibration energy reduction, at the same time, the increasing stiffness of fastener and rubber pad can reduce the vibration energy, and the effect is higher than increasing the damping. Meanwhile, changing the stiffness of the sleeper rubber pad has the greatest impact on the vibration level of rail, sleeper, and the surface soil. The changing stiffness of the fastener has great influence on the vibration level of rail and sleeper, while a certain impact will happen on the vibration level of the system when the damping of the fastener and sleeper rubber pad changed, but it is relatively small to the change of stiffness.

(3) During the operation of the metro vehicle, the vibration energy continuously decays pass through rail, sleeper, the tunnel lining, and finally the soil,

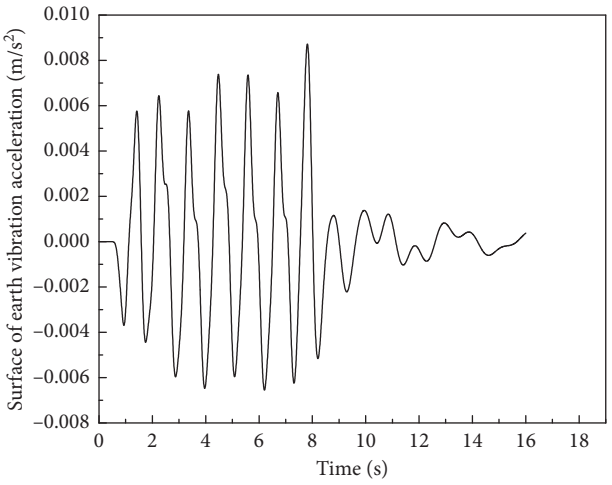


Figure 17: The time history of the acceleration.

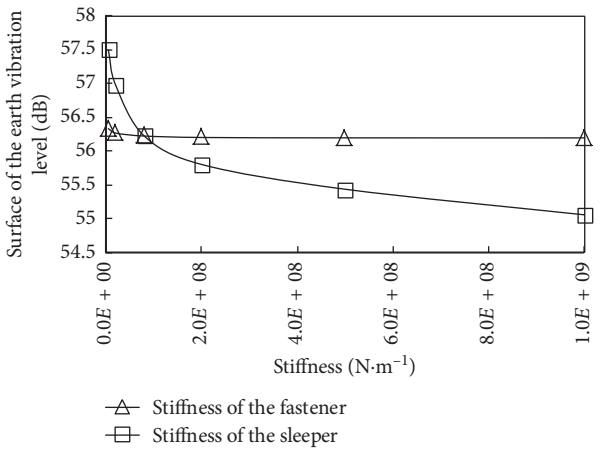


Figure 18: The influence of stiffness change on the vibration power level.

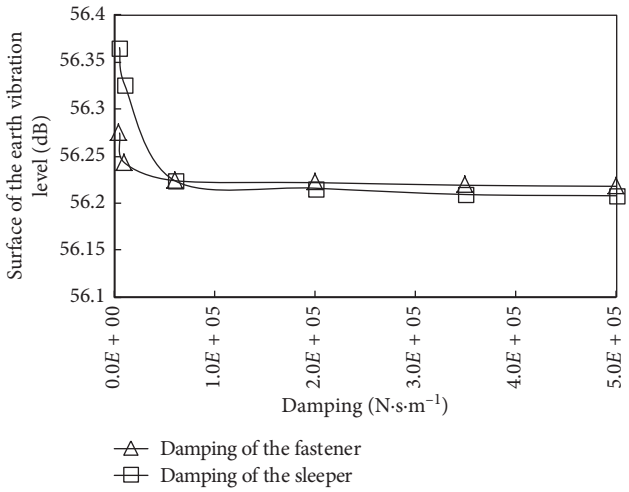


Figure 19: The influence of damping change on the vibration power level.

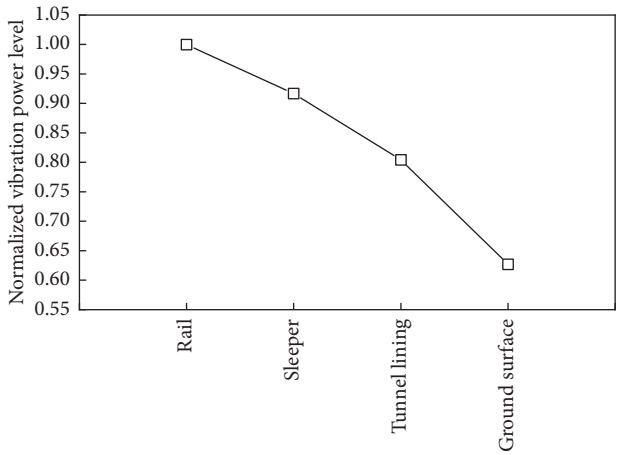


Figure 20: The attenuation of vibration energy in the system.

and eventually, vibration energy reaching the surface is only 62% of the rail vibration energy.

## Data Availability

The data used to support the findings of this study are available from the corresponding author upon request.

## Conflicts of Interest

The authors declare that they have no conflicts of interest.

## Acknowledgments

The National Natural Science Foundation of China (no. 51278099) supported this work.

## References

[1] Z. M. Schrag, *The Great Society Subway: A History of the Washington Metro*, JHU Press, Baltimore, MD, USA, 2014.

[2] S. Guo, H. Luo, and L. Yong, "A big data-based workers behavior observation in China metro construction," *Procedia Engineering*, vol. 123, pp. 190–197, 2015.

[3] S. Timoshenko, "Method of analysis of statical and dynamical stresses in rail," in *Proceedings of the 2nd International Congress for Applied Mechanics*, pp. 12–17, Zurich, Switzerland, September 1926.

[4] L. Xu, W. Zhai, and J. Gao, "A probabilistic model for track random irregularities in vehicle/track coupled dynamics," *Applied Mathematical Modelling*, vol. 51, pp. 145–158, 2017.

[5] E. Aggestam, J. C. O. Nielsen, and R. Bolmsvik, "Simulation of vertical dynamic vehicle-track interaction using a two-dimensional slab track model," *Vehicle System Dynamics*, vol. 56, no. 11, pp. 1633–1657, 2018.

[6] P. Lopes, J. F. Ruiz, P. A. Costa, L. Medina Rodríguez, and A. Silva Cardoso, "Vibrations inside buildings due to subway railway traffic. Experimental validation of a comprehensive prediction model," *Science of the Total Environment*, vol. 568, pp. 1333–1343, 2016.

[7] L. Ling, J. Han, X. Xiao, and X. Jin, "Dynamic behavior of an embedded rail track coupled with a tram vehicle," *Journal of Vibration and Control*, vol. 23, no. 14, pp. 2355–2372, 2017.

[8] Y. Qi, H. Dai, J. Yang, and K. Xu, "Dynamic analysis of vehicle track coupling based on double beam track model," *Shock and Vibration*, vol. 2018, Article ID 7469894, 10 pages, 2018.

[9] L. Xu and W. Zhai, "A new model for temporal–spatial stochastic analysis of vehicle–track coupled systems," *Vehicle System Dynamics*, vol. 55, no. 3, pp. 427–448, 2017.

[10] W. Zhai, K. Wang, and C. Cai, "Fundamentals of vehicle-track coupled dynamics," *Vehicle System Dynamics*, vol. 47, no. 11, pp. 1349–1376, 2009.

[11] X. Lei and N. A. Noda, "Analyses of dynamic response of vehicle and track coupling system with random irregularity of track vertical profile," *Journal of Sound and Vibration*, vol. 258, no. 1, pp. 147–165, 2002.

[12] Y. Q. Sun and M. Dhanasekar, "A dynamic model for the vertical interaction of the rail track and wagon system," *International Journal of Solids and Structures*, vol. 39, no. 5, pp. 1337–1359, 2002.

[13] J. A. Forrest and H. E. M. Hunt, "A three-dimensional tunnel model for calculation of train-induced ground vibration," *Journal of Sound and Vibration*, vol. 294, no. 4, pp. 678–705, 2006.

[14] X. Bian, W. Jin, and H. Jiang, "Ground-borne vibrations due to dynamic loadings from moving trains in subway tunnels," *Journal of Zhejiang University SCIENCE A*, vol. 13, no. 11, pp. 870–876, 2012.

[15] S. Gupta, M. F. M. Hussein, G. Degrande, H. E. M. Hunt, and D. Clouteau, "A comparison of two numerical models for the prediction of vibrations from underground railway traffic," *Soil Dynamics and Earthquake Engineering*, vol. 27, no. 7, pp. 608–624, 2007.

[16] W. Shi, L. Miao, Z. Wang, and J. Luo, "Settlement behaviors of metro tunnels during the metro operation," *Shock and Vibration*, vol. 2015, Article ID 863961, 11 pages, 2015.

[17] P. Amado-Mendes, P. Alves Costa, L. M. C. Godinho, and P. Lopes, "2.5D MFS–FEM model for the prediction of vibrations due to underground railway traffic," *Engineering Structures*, vol. 104, pp. 141–154, 2015.

[18] A. El Kacimi, P. K. Woodward, O. Laghrouche, and G. Medero, "Time domain 3D finite element modelling of train-induced vibration at high speed," *Computers & Structures*, vol. 118, pp. 66–73, 2013.

[19] W. Gardien and H. G. Stuit, "Modelling of soil vibrations from railway tunnels," *Journal of Sound and Vibration*, vol. 267, no. 3, pp. 605–619, 2003.

[20] T. Ekevid, H. Lane, and N. E. Wiberg, "Adaptive solid wave propagation-influences of boundary conditions in high-speed train applications," *Computer Methods in Applied Mechanics and Engineering*, vol. 195, no. 4, pp. 236–250, 2006.

[21] S. H. Ju, "Finite element investigation of traffic induced vibrations," *Journal of Sound and Vibration*, vol. 321, no. 3, pp. 837–853, 2009.

[22] L. Andersen and C. J. C. Jones, "Coupled boundary and finite element analysis of vibration from railway tunnels—a comparison of two- and three-dimensional models," *Journal of Sound and Vibration*, vol. 293, no. 3–5, pp. 611–625, 2006.

[23] T. Real, C. Zamorano, F. Ribes, and J. I. Real, "Train-induced vibration prediction in tunnels using 2D and 3D FEM models in time domain," *Tunnelling and Underground Space Technology*, vol. 49, pp. 376–383, 2015.

[24] K. Vogiatzis, "Environmental ground borne noise and vibration protection of sensitive cultural receptors along the Athens Metro Extension to Piraeus," *Science of the Total Environment*, vol. 439, pp. 230–237, 2012.

[25] Y. Tang, H. Zhao, Y. Wang et al., "Characteristics of strain accumulation of reinforced soft clay around tunnel under subway vibration loading," *Journal of Tongji University*, vol. 39, no. 7, pp. 972–977, 2011.

[26] S. G. Newton and R. A. Clark, "An investigation into the dynamic effects on the track of wheelflats on railway vehicles," *Journal of Mechanical Engineering Science*, vol. 21, no. 4, pp. 287–297, 1979.

[27] S. Timoshenko, *Vibration Problems in Engineering*, John Wiley & Sons, Hoboken, NJ, USA, 4th edition, 1974.

[28] Z. Shijian, J. Lou, and Q. He, *Vibration Theory and Vibration Isolation Technology*, National Defense Industry Press, Beijing, China, 2006.

[29] Z. Y. Shen, J. K. Hedrick, and J. A. Elkins, "A comparison of alternative creep force models for rail vehicle dynamic analysis," *Vehicle System Dynamics*, vol. 12, no. 1–3, pp. 79–83, 1983.

[30] J. A. Priest and W. Powrie, "Determination of dynamic track modulus from measurement of track velocity during train passage," *Journal of Geotechnical and Geoenvironmental Engineering*, vol. 135, no. 11, pp. 1732–1740, 2009.

[31] International Standard, *Mechanical Vibration and Shock Evaluation of Human Exposure to Whole-Body Vibration, ISO 2631-1*, Vol. 5, International Organization for Standardization, Geneva, Switzerland, 1997.

[32] X. Sun, *Prediction of Environment Vibrations Induced by Metro Trains and Mitigation Measures Analysis*, Beijing Jiaotong University, Beijing, China, 2008.

[33] F. Kang and J. Zhang, *The Application of ABAQUS in Geotechnical Engineering*, China Water & Power Press, Beijing, China, 2010.

[34] B. O. Hardin and V. P. Drnevich, "Shear modulus and damping in soils: design equations and curves," *Journal of Soil Mechanics and Foundations Division*, vol. 98, no. 7, pp. 667–692, 1972.